

# Fluctuating dynamics at the quasiperiodic onset of chaos, Tsallis $q$ -statistics and Mori's $q$ -phase thermodynamics

H. Hernandez-Saldana and A. Robledo<sup>y</sup>

Instituto de Física,

Universidad Nacional Autónoma de México,

Apartado Postal 20-364, México 01000 D.F., México.

(Dated: .)

We analyze the fluctuating dynamics at the golden-mean transition to chaos in the critical circle map and find that trajectories within the critical attractor consist of infinite sets of power laws mixed together. We elucidate this structure assisted by known renormalization group (RG) results. Next we proceed to weigh the new findings against Tsallis' entropic and Mori's thermodynamic theoretical schemes and observe behavior to a large extent richer than previously reported. We find that the sensitivity to initial conditions  $\epsilon_t$  has the form of families of intertwined  $q$ -exponentials, of which we determine the  $q$ -indexes and the generalized Lyapunov coefficient spectra  $\lambda_q$ . Further, the dynamics within the critical attractor is found to consist of not one but a collection of Mori's  $q$ -phase transitions with a hierarchical structure. The value of Mori's 'thermodynamic field' variable  $q$  at each transition corresponds to the same special value for the entropic index  $q$ . We discuss the relationship between the two formalisms and indicate the usefulness of the methods involved to determine the universal trajectory scaling function and/or the occurrence and characterization of dynamical phase transitions.

PACS numbers: 05.45.Ac, 05.90.+m, 05.10.Lc

## I. INTRODUCTION

The unfamiliar dynamics at critical attractors of even the standard one dimensional nonlinear iterated maps [1]–[3] is of current interest to statistical physicists; it provides insights into properties of systems at which the key supports of the canonical theory, phase space mixing and ergodicity, break down. At these attractors the indicators of chaos withdraw, such as the fast rate of separation of initially close-by trajectories. There is a small number of known routes to chaos and it is of interest to know if at their thresholds the dynamics displays similar features and if so to what extent. If present, these similarities would apply above the known universality of each type of critical attractor.

Critical attractors of nonlinear low-dimensional maps have always drawn much interest because they demonstrate the ways by which nonlinear systems bridge periodic and chaotic motion [1]–[3]. The geometrical properties of these attractors have been known for a long time [1]–[3], but their dynamical properties are even now perplexing and still need to be fully understood. Renewed interest in this subject [4] – [15] has focused on the applicability of  $q$ -statistics, the generalization of the Boltzmann-Gibbs (BG) statistical mechanics proposed by Tsallis [16], [17], to these nonlinear systems. Important examples of critical attractors are the onset of chaos via period doubling, intermittence and quasiperiodicity, the three universal routes to chaos in dissipative maps

displayed by the prototypical logistic and circle maps [1] – [3]. Perhaps the most interesting types of critical attractors are critical strange nonchaotic attractors [18] as in the period doubling and quasiperiodic onset of chaos. These are geometrically complicated multifractal attractors with a vanishing Lyapunov coefficient  $\lambda_1$  and a sensitivity to initial conditions  $\epsilon_t$  that does not converge to any single-valued function but instead displays a fluctuating pattern that grows as a power law in time  $t$  [19] – [23].

Trajectories within a critical attractor show self-similar temporal structures, they preserve memory of their previous locations and do not have the mixing property of truly chaotic trajectories [23]. A special version of the 'thermodynamic formalism' was adapted long ago [20]–[23] to study the dynamics at critical attractors and quantitative results were obtained that provided a first understanding, particularly about the envelope of the fluctuating  $\epsilon_t$  and the occurrence of a so-called ' $q$ -phase' dynamical phase transition [21] – [23]. As shown below we uncover a complete and rich dynamical structure for  $\epsilon_t$  and clarify its relationship to families of  $q$ -phase transitions. We explain how these transitions relate to distinct regions of the multifractal attractor, and their manifestation in the universal jump discontinuities of the trajectory scaling function [24] – [26]. We clarify also the relationship of the thermodynamic approach with  $q$ -statistics with regards to the dynamical properties studied.

Recently, rigorous results have been developed [8]–[15] that support the validity of  $q$ -statistics (outlined in the next paragraph) for the critical attractors associated with the intermittency and period-doubling routes to chaos, i.e. the tangent bifurcation and the accumulation point of the pitchfork bifurcations, but studies of the same type

<sup>E</sup>lectronic address: hugo@fisica.unam.mx

<sup>y</sup>Electronic address: robledo@fisica.unam.mx

have not been carried out for the quasiperiodic route to chaos. Here we present results on this route by considering the proverbial golden-mean onset of chaos in the critical circle map [1], [3] and show that there are elements of universality in their dynamical properties as they appear in close correspondence with those recently analyzed for the Feigenbaum attractor [15].

The central point of the  $q$ -statistics with regards to the description of the dynamics of critical attractors is a sensitivity to initial conditions  $\epsilon_t$  related to the  $q$ -exponential functional form, i.e. the 'q-deformed' exponential function  $\exp_q(x) = [1 - (q-1)x]^{1/(q-1)}$  [4], [5]. From such  $\epsilon_t$  one or more spectra of  $q$ -generalized Lyapunov coefficients  $\lambda_q$  can be determined [9], [15]. The  $\lambda_q$  are dependent on the initial position and each spectrum can be examined by varying this position. The  $\lambda_q$  satisfy an identity  $\lambda_q = K_q$  where  $K_q$  is an entropy production rate based on the Tsalis entropy  $S_q$ , defined in terms of the  $q$ -logarithmic function  $\ln_q y = (y^{1-q} - 1)/(1-q)$ , the inverse of  $\exp_q(x)$  [4], [9], [15].

Here we find that  $\epsilon_t$  at the golden-mean onset of chaos takes the form of a family of interwoven  $q$ -exponentials. The  $q$ -indexes appear in conjugate pairs,  $q$  and  $Q = 2 - q$ , as these correspond to switching starting and finishing trajectory positions. We show that  $q$  and  $Q$  are related to the occurrence of pairs of dynamical  $q$ -phase transitions that connect qualitatively different regions of the attractor [21] - [23]. These transitions are identified as the source of the special values for the entropic index  $q$ , and these values are determined by the universality class parameters to which the attractor belongs. In our present case the parameters are the golden-mean winding number  $w_{gm} = (\sqrt{5} - 1)/2 = 2'0:618034$  and the universal constants (in the sense of Feigenbaum's trajectory scaling function [24] - [26]) that measure the power-law clustering of iterate positions. The most prominent of the universal constants is  $\delta_{gm} = 1.288575$ , that appears in the description of the most rarefied region and (as  $\delta_{gm}^{-3}$ ) of the most crowded region of the multifractal attractor.

We are interested here in determining the detailed dependence of the aforementioned dynamical structure for the golden-mean chaos threshold on both the initial position and the observation time  $t$  as this dependence is preserved by the infinite memory of trajectories. To this purpose we recall in the following Section 2 the familiar features of the circle map, and the properties of the renormalization group (RG) fixed-point map for a cubic inflection point with zero slope. Then in Section 3 we describe the organization of the superstable trajectory at the chaos threshold into families of positions that lie along power laws in time. Assisted by these properties, in Section 4 we determine the sensitivity  $\epsilon_t$  for trajectories that have their starting and finishing positions at the most crowded and most sparse regions of the multifractal attractor. In Section 5 we explain how the properties for  $\epsilon_t$  and its  $\lambda_q$  spectrum are related to the occurrence of dynamical  $q$ -phase transitions and corroborate previously obtained numerical results. In Section 6 we express

$\epsilon_t$  in terms of the discontinuities of the trajectory scaling function that measures local contraction rates within the multifractal attractor. From this relationship we obtain results for trajectories that involve other multifractal regions and show that the dynamics consists of a hierarchy of  $q$ -indexes and  $q$ -phase transitions. In Section 7 we summarize our results and further discuss the links between the thermodynamic and  $q$ -statistical schemes and call attention to the usefulness of the latter.

## II. THE GOLDEN-MEAN ONSET OF CHAOS

To assist our presentation in the following sections we recall here basic features of the circle map [1], [3]. The map is given by

$$f_K(\theta) = \theta + K \sin 2\pi\theta \pmod{1}; \quad (1)$$

where the control parameters  $\theta$  and  $K$  are the bare winding number and the amount of nonlinearity, respectively. An important parameter for the description of the structure of the trajectories of this map is the dressed winding number

$$w = \lim_{t \rightarrow \infty} \frac{\langle t \rangle - \langle 0 \rangle}{t}; \quad (2)$$

the average increment of  $\langle t \rangle$  per iteration. The map is monotonic and invertible for  $K < 1$ , develops a cubic inflection point at  $\theta = 0$  (or  $\theta = 1$ , see Figs. 1) for  $K = 1$ , and becomes nonmonotonic and noninvertible for  $K > 1$ . For  $K < 1$  trajectories are periodic (locked motion) when  $w$  is rational and quasiperiodic (unlocked motion) when  $w$  is irrational. The winding number  $w(\theta)$  forms a 'devil's staircase' making a step at each rational  $p/q$  and remaining constant  $w = p/q$  for a range of  $\theta$ . For  $K = 1$ , the critical circle map, locked motion covers the entire interval leaving only a multifractal set of unlocked. The threshold to chaos is obtained at the accumulation points of sequences of control parameter values of families of periodic trajectories. At these accumulation points the trajectories are quasiperiodic. For  $K > 1$  the regions of periodic motion (Arnold tongues) overlap leading to chaotic motion.

A standard way to study the quasiperiodic route to chaos is to fix the value of  $K = 1$  and select an irrational  $w$ . Then a choice is made of successive rational values for  $\theta$  to obtain an infinite sequence of winding numbers that approach  $w$ . A convenient sequence of such rational values for  $\theta$  are given by consecutive truncations of the continued fraction expansion of  $w$ . A well-studied, and perhaps the most interesting, case is the sequence of rational approximants to  $w_{gm} = (\sqrt{5} - 1)/2 = 2'0:618034$ , the reciprocal of the golden mean, that yields the winding numbers  $w_n = F_{n-1}/F_n$ , where  $F_n$  are the Fibonacci numbers  $F_{n+1} = F_n + F_{n-1}$ . Within the range of  $\theta$  for which  $w = F_{n-1}/F_n$  one observes trajectories of period  $F_n$ , and therefore a route to chaos consists of an infinite

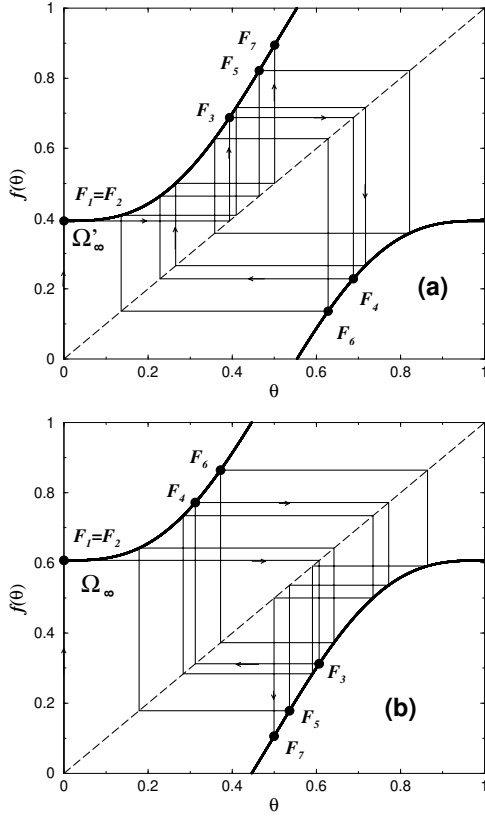


FIG. 1: Critical circle map  $K = 1$  and supercycle trajectories. a)  $\frac{0}{1}$ . b)  $\frac{1}{1}$ . The labels  $F_n$  correspond to trajectory times given by Fibonacci numbers.

family of periodic orbits with increasing periods of values  $F_n, n \geq 1$ . It has proved useful to single out from these families the periodic trajectories with the 'superstable' property. We recall that a superstable orbit [1], [3] is an orbit of period  $T$  such that  $df^T(\theta) = d = 0$ . In our case a superstable orbit is one that contains as one of its positions  $\theta = 0$ . Since the derivative of  $f_{n+1}(\theta)$  at  $\theta = 0$  vanishes the Lyapunov coefficient  $\lambda_1$  diverges to  $\infty$  for these family of orbits. The values of  $\theta_n, n = 1; 2; \dots$ , at which they occur can be determined from their definition when written as  $f_{n+1}^{\theta_n}(0) = F_n, n = 1; 2; \dots$ . The solutions of this equation lie on zigzag paths approaching the limit  $\theta_1 \approx 0.606661$  which corresponds to  $w_{gm}$ . As the golden mean  $w_{gm}$  arises from the condition  $w = 1 - w^2$ , a second superstable family of trajectories is determined by considering the winding numbers  $w_n^0 = F_{n+2} = F_n$ , with  $\theta_n^0, n = 1; 2; \dots$ , obtained in turn from  $f_{n+1}^{\theta_n^0}(0) = F_{n+1}$ . The  $\theta_n^0$  converge to  $\theta_1^0 = 1 - \theta_1 \approx 0.393339$  which corresponds to  $w_{gm}^2 \approx 0.381966$ . In Figs. 1a and 1b we show the critical map for  $\frac{0}{1}$  and  $\frac{1}{1}$ , respectively, together with a portion of the superstable trajectory at the chaos threshold. In Fig. 2 we show the values for the Lyapunov coefficients  $\lambda_1$  for  $K = 1$  as a function of  $\Omega$  where the locations of the two superstable families are clearly seen and those for their accumulation points are

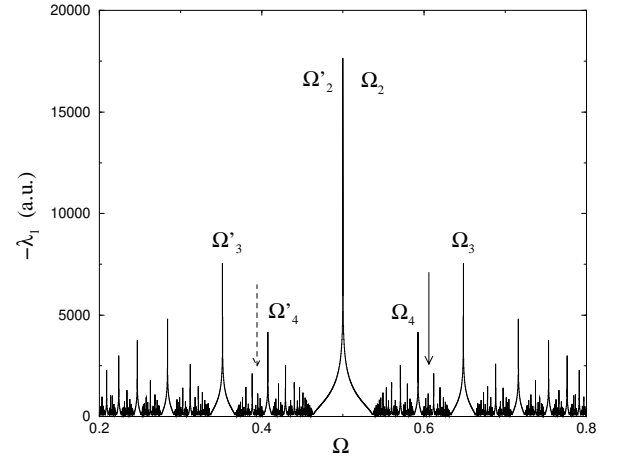


FIG. 2: The Lyapunov coefficient  $\lambda_1$  for the critical circle map  $K = 1$  as a function of winding number. The supercycle divergences to  $\infty$  can be clearly appreciated and the locations for the two accumulation points at  $\frac{0}{1}$  and  $\frac{1}{1}$  are indicated by the arrows.

indicated.

A celebrated development [1], [3] dating from the early 80's is the recognition that the quasiperiodic route to chaos displays universal scaling properties. The analysis was based on an RG approach analogous to that for the period doubling cascade, and can be suitably discussed in terms of the critical circle map. The universal properties are obtained from the fixed-point map  $g(\cdot)$  of an RG transformation that consists of functional composition and rescaling appropriate for maps with a zero-slope cubic inflection point. The fixed-point map satisfies

$$g(\cdot) = g_{gm} g(g_{gm} g(\cdot) = \frac{2}{g_{gm}}); \quad (3)$$

where  $g_{gm} \approx 1.288575$  is a universal constant [1], [3]. This constant describes the scaling of the distance  $d_n$  from  $\theta = 0$  to the nearest element of the orbit with  $w_n$ , i.e.  $d_n = f_{n+1}^{\theta_n}(0) - F_{n+1}$ . The scaling is given by  $\lim_{n \rightarrow \infty} (d_n/d_{n+1}) = g_{gm}$ . Related to the chaos threshold at the golden mean  $w_{gm}$  there is a multifractal set (the attractor) that measures the different degrees of clustering of iterate positions. This multifractal has a dimension spectrum  $f(\cdot)$  within a range of values between  $m_{min}$  and  $m_{max}$  [27]. The most rarefied region of the multifractal corresponds to  $m_{max} = \ln w_{gm} = \ln j_{gm} \approx 1.897995$ , and this region is mapped onto the multifractal's most crowded region characterized by  $m_{min} = -\ln w_{gm} = 3 \ln j_{gm} \approx 0.632665$  [27]. The chaos threshold for special values of the winding number is known as local universality [1].

### III. STRUCTURE OF TRAJECTORIES WITHIN THE ATTRACTOR

We consider the last of the superstable trajectories, with infinite period when  $\mu = 1$  or  $\frac{0}{1}$  and starting at  $\theta(0) = 0$ . As we shall see all other trajectories within the attractor can be obtained from it. We find it convenient to plot the positions  $\theta(t)$  and their iteration time  $t$  in logarithmic scales as shown in Figs. 3a and 3b, obtained for  $\mu = 1$  and  $\frac{0}{1}$ , respectively, and where the labels record the times at which positions are reached. A distinctive feature in these figures is that positions fall along straight diagonal lines, an indication of embedded power law behavior. Notice that the positions of the main diagonal in Fig. 3a correspond to the times  $F_{2n}$ ,  $n = 1; 2; 3; \dots$ . The succeeding diagonals above it appear grouped together. Above the main diagonal there are  $k = 2$  close-by diagonals the first with positions that correspond to times of the form  $2F_{2n}$  and the second for times of the form  $F_{2n} + F_{2n-2}$ . Above these two diagonals there is a group of  $k = 3$  diagonals and above them a group of  $k = 4$ , etc. The times for the positions along each diagonal in the group of  $k$  diagonals are, from the bottom to the top, of the form  $kF_{2n}$ ,  $(k-1)F_{2n} + F_{2n-2}$ ,  $(k-2)F_{2n} + 2F_{2n-2}$ , ...,  $F_{2n} + (k-1)F_{2n-2}$ ,  $n = 1; 2; 3; \dots$ . The same structure is observed in Fig. 3b with  $F_{2n}$  replaced by  $F_{2n+1}$ . The slope shared by all the diagonal straight lines in Figs. 3a and 3b is  $-\ln j_{gm} = -\ln w_{gm}$ . Note too that the positions for  $F_{2n}$  in Fig. 3a appear along the top of Fig. 3b and approach asymptotically the horizontal line  $\theta = 1$ . And vice versa, the positions for  $F_{2n+1}$  in Fig. 3b appear along the top of Fig. 3a and approach asymptotically the horizontal line  $\theta = 1$ . Analogous features hold for the positions of the groups of subsequences with  $k > 1$ . A similar pattern of time subsequence positions arranged along parallel decreasing straight lines is observed in the plot of  $\ln j_1(t)$  vs  $\ln t$  (or identically,  $\ln j_1(t)$  vs  $\ln t$ ) that is shown in Fig. 4. As it can be observed there, the power-law diagonals along which positions fall appear again arranged in groups, each with an increasing number of members  $k = 1; 2; 3; \dots$ . The times for the positions along the group of  $k$  diagonals are, from the bottom to the top, of the form  $kF_n + 1$ ,  $(k-1)F_n + F_{n-2} + 1$ ,  $(k-2)F_n + 2F_{n-2} + 1$ , ...,  $F_n + (k-1)F_{n-2} + 1$ ,  $n = 1; 2; 3; \dots$ , and the slope shared by all the diagonals is  $-3 \ln j_{gm} = -\ln w_{gm}$ .

More speci cally, the trajectory starting at  $\theta(0) = 0$  maps out the attractor in such a way that the values of succeeding (time-shifted  $= t + 1$ ) positions form subsequences with a common power-law decay of the form  $\theta^{1-Q}$  with  $Q = 1 - \ln j_{gm} = -\ln j_{gm}' = 2.897995$ . (To avoid confusion we denote as  $\theta(t)$  position at time  $t$  and as  $\theta(t+1)$  the same position at shifted time  $t+1$ ). That is, the entire attractor can be decomposed into position subsequences generated by the time subsequences  $t = (k-1)F_n + 1$ , each obtained by running over  $n = 1; 2; 3; \dots$  for fixed values of  $k = 1; 2; 3; \dots$  and  $l = 0; 1; 2; \dots; k-1$ . Noticeably, the positions for these

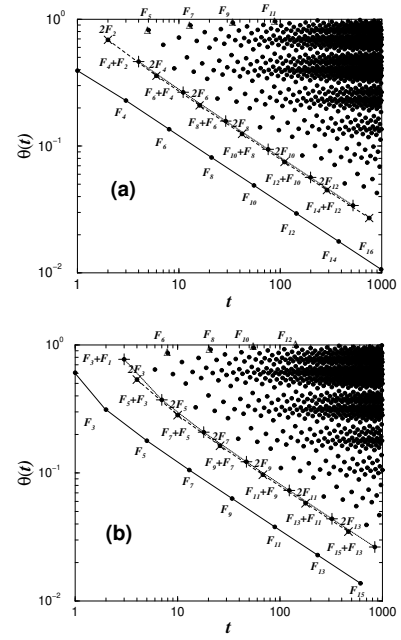


FIG. 3: a) Positions  $\theta(t)$  vs  $t$  in logarithmic scales for the orbit with initial condition  $\theta(0) = 0$  at  $\frac{0}{1}$  of the critical circle map  $K = 1$ . The lines are guides to the eye. The labels indicate iteration time  $t$ , the dashed line and symbols  $+$  correspond to times of the form  $2F_{2n}$ , and the dotted line and symbols  $+$  correspond to times of the form  $F_{2n} + F_{2n-2}$ . The symbols  $\circ$  correspond to the main diagonal positions at  $F_{2n+1}$  in (b). b) Same as a) with  $\frac{0}{1}$  replaced by  $\frac{1}{1}$ . The dashed line and symbols  $+$  correspond to times of the form  $2F_{2n+1}$ , and the dotted line and symbols  $+$  correspond to times of the form  $F_{2n+1} + F_{2n-1}$ . The symbols  $\circ$  correspond to the main diagonal positions at  $F_{2n}$  in (a). See text for description.

subsequences can be asymptotically obtained from those belonging to the superstable periodic orbits of lengths  $F_n$  at  $\mu = 1$  or  $\frac{0}{1}$ . In particular, the positions for the main subsequence  $k = 1$ , that constitutes the lower bound of the entire trajectory, can be identified to be  $F_n' = j_{gm}^n$ ,  $n = 1, 2, 3, \dots$ . The positions for each time subsequence that leads a group,  $k > 1$  and  $l = 0$ , i.e.  $t = kF_n$  in Figs. 3 can be expressed, when use is made of the time shift  $t = t + k$  and

$$\frac{F_n}{F_{n-1}} \frac{F_{n-1}}{F_{n-2}} \cdots \frac{F_2}{F_1} = w_{gm}^n; \quad (4)$$

as

$$\theta = k \exp_{Q_+} \left( \frac{(k)}{Q_+} t \right); \quad (5)$$

with  $Q_+ = 1 - \ln j_{gm} = -\ln j_{gm}'$  and  $\frac{(k)}{Q_+} = -\ln j_{gm} - k \ln w_{gm}$ . The same time subsequence positions given by  $t = kF_n + 1$  in Fig. 4 can be expressed as

$$j_1(t) = j_1(t - k) \exp_{Q_+} \left( \frac{(k)}{Q_+} t \right); \quad (6)$$

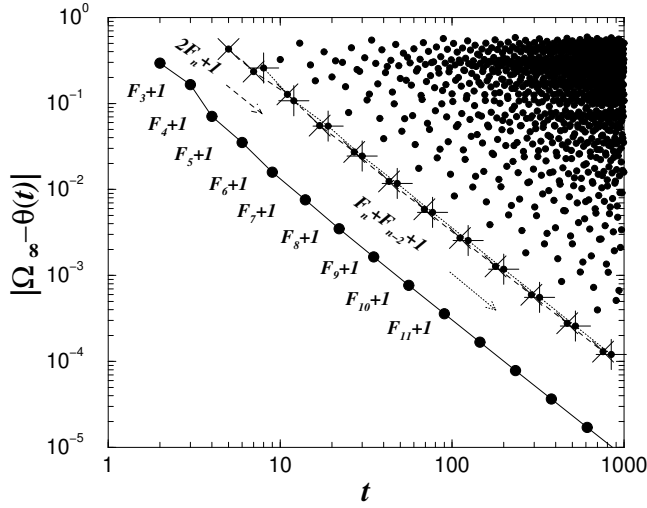


FIG. 4: Positions  $j_1(t)$  just in logarithmic scales for the orbit with initial condition  $(0) = 0$  at  $t_1$  of the critical circle map  $K = 1$ . The labels indicate iteration time  $t$ . The dashed line and symbols  $\times$  correspond to times of the form  $2F_n + 1$ , and the dotted line and symbols  $+$  correspond to times of the form  $F_n + F_{n-2} + 1$ . The same results are obtained with  $t_1$  replaced by  $\frac{0}{1}$ . See text for description.

with  $Q = 1$ ,  $\ln w_{gm} = 3 \ln j_{gm}$  and  $\frac{(k)}{Q} = 3 \ln j_{gm} j = k \ln w_{gm}$ . Interestingly, these results can be seen to satisfy the dynamical scaling relation,

$$h = \frac{1}{1-Q} g\left(\frac{1}{1-Q}\right) \quad (7)$$

with  $h = \frac{1}{Q}$  or  $j_1$  where  $j = kw_{gm}^n$  with  $w_{gm} = \frac{1}{Q}$  or  $w_{gm} = \frac{3(1-Q)}{Q}$ , and where  $g$  is the fixed-point map with  $j = k$  or  $j_1$ . The similarities with the dynamical properties of the supercycle orbit  $2^1$  at the Feigenbaum attractor are remarkable, see Refs. [8], [9] for the quadratic map and Refs. [10], [15] for its generalization to general nonlinearity  $z > 1$ .

#### IV. SENSITIVITY TO INITIAL CONDITIONS

We have now elements to derive the sensitivity to initial conditions  $t_k(0)$ , defined as  $t_k(0) = d(t)/d(0)$ , when either  $(0) = 0$  or  $(0) = 1$ . For simplicity of presentation we consider the case of the leading position subsequences within each group  $k$ , those for times  $t = kF_n$  as described in the previous section. The results for the other subsequences within each group are similar and we only quote the differences in the expressions. We proceed in the following way. Recall [28] that

$$f_n(\cdot) = \frac{n}{gm} g\left(\frac{n}{gm}\right); \quad n \geq 0; \quad (8)$$

where  $f_n(\cdot) = \frac{F_n}{F_{n+1}}(\cdot) = F_{n+1}$ , and consider the lower-order terms in the expansion of  $g\left(\frac{n}{gm}\right)$ , i.e.

$$g\left(\frac{n}{gm}\right) = g(0) + \frac{1}{6} g'''(0) \left(\frac{3n}{gm}\right)^3; \quad (9)$$

If we denote the starting positions of two nearby trajectories at time  $t = k$  by

$$j_k = f_1(\cdot) = g(0) + \frac{1}{6} g'''(0) \left(\frac{3}{6}\right)^3 \quad (10)$$

and

$$j_k = f_1(\cdot) = g(0) + \frac{1}{6} g'''(0) \left(\frac{3}{6}\right)^3; \quad (11)$$

their positions at time  $t = kF_n$  are given by

$$j_{kF_n} = f_n(\cdot) = \frac{n}{gm} g(0) + \frac{1}{6} g'''(0) \left(\frac{2n}{gm}\right)^3 \quad (12)$$

and

$$j_{kF_n} = f_n(\cdot) = \frac{n}{gm} g(0) + \frac{1}{6} g'''(0) \left(\frac{2n}{gm}\right)^3; \quad (13)$$

From the above we obtain

$$\frac{j_{kF_n}}{j_k} = \frac{j_{kF_n}}{j_k} = j_{gm}^{2n}; \quad n \geq 1; \quad (14)$$

where we have used the equality sign in consideration of the scaling limit for large  $n$ . For each subsequence  $k$ , the sensitivity  $t_k$ , given for the trajectories considered by

$$t_k(k) = \lim_{j_k \rightarrow 0} \frac{j_k}{j_k}; \quad (15)$$

can be written, with use of the shifted time variable  $t_k$ , and observing that

$$j_{gm}^{2n} = 1 + \frac{t_k}{k}; \quad (16)$$

as the  $q$ -exponential

$$t_k(k) = \exp_q \left( \frac{1}{q} t_k \right); \quad (17)$$

where

$$q = 1 + \frac{\ln w_{gm}}{2 \ln j_{gm} j}; \quad 0.051003 \quad (18)$$

and

$$\frac{(k)}{q} = 2 \frac{\ln j_{gm} j}{k \ln w_{gm}}; \quad (19)$$

The value of  $q$  in Eq. (18) agrees with that obtained in earlier studies [5]–[7].

The departing positions,  $(0) = 0$  (or  $(0) = 1$ ), for  $t_k$  in Eq. (17) are located in the most crowded region of the attractor and the value of  $k$  in  $\frac{(k)}{q}$  in Eq. (17) locates this position as the top position with time label  $t = kF_1 = k$  of the subsequences described by the times  $t = kF_n$  in Figs. 3a and 3b. By construction, the observation times in Eq. (17) are precisely  $t = kF_n$  when

the iterate is close to the most sparse region of the attractor,  $x_0' = 1$  (or  $x_0' = 0$ ). The sensitivity  $t_{+1}$  for the inverse trajectories, with departing positions at the most sparse region and with observation times when at the most crowded region, can be evaluated in the same way as above, with the result

$$t_{+1} = \exp_{2-q} \frac{h}{2-q} \frac{i}{2-q} t; \quad (20)$$

with  $q$  as above and where

$$\frac{(k)}{2-q} = \frac{2 \ln j_{gm}}{k w_{gm} \ln w_{gm}}; \quad (21)$$

Trajectories expand in one direction and contract in the opposite one. We recall that  $\exp_q(x) = 1 = \exp_{2-q}(-x)$ . The factor of  $w_{gm}^{-1}$  in  $\frac{(k)}{2-q}$  appears because of a basic difference between the orbits of periods  $F_n$  and  $F_1$ . In the latter case, to reach  $(t^0)' = 0$  from  $(0)' = 1$  at times  $t^0 = F_n + 1$  the iterate necessarily moves into positions of the next period  $F_{n+1}$ , and orbit contraction is  $w_{gm}^{-1}$  as effective than expansion. When considering the other sets of positions within each group of subsequences one obtains the same results as in Eqs. (17) to Eq. (21) with  $k$  replaced by  $(k-1) + \ln w_{gm}^2$  in Eqs. (19) and (21).

#### V. MORI'S $q$ -PHASE TRANSITIONS AND TSALLIS' $q$ INDEX

About 15 years ago Mori and coworkers developed a broad thermodynamic formalism to characterize sharp changes at bifurcations and at other singular attractors in low dimensional maps [23]. The formalism was specially adapted to study critical attractors and was applied to the specific case of the onset of chaos in the circle map at the golden mean [21], [23] and in the logistic map at the period doubling accumulation point [22], [23]. For critical attractors the scheme involves the evaluation of fluctuations of the generalized finite-time Lyapunov coefficient

$$(t; x_0) = \frac{1}{\ln t} \sum_{i=0}^{X-1} \ln \frac{df(x_i)}{dx_i}; \quad t \geq 1; \quad (22)$$

where  $f(x)$  is a map with control parameter(s) tuned at a critical attractor. Notice the replacement of the customary  $t$  by  $\ln t$  in Eq. (22), as the ordinary Lyapunov coefficient  $\lambda_1$  vanishes for critical attractors at  $t \rightarrow 1$ .

The density distribution for the values of  $\lambda$ , at  $t \rightarrow 1$ ,  $P(\lambda; t)$ , is written in the form [23], [21], [22]

$$P(\lambda; t) = t^{-(1)} P(0; t); \quad (23)$$

where  $(\cdot)$  is a concave spectrum of the fluctuations of  $\lambda$  with minimum  $(0) = 0$  and is obtained as the Legendre transform of the 'free energy' function  $(q)$ , defined

as  $(q) = \lim_{t \rightarrow 1} \frac{1}{t} \ln Z(t; q) = \ln t$ , where  $Z(t; q)$  is the dynamic partition function

$$Z(t; q) = \int dP(\lambda; t) t^{(q-1)\lambda}; \quad (24)$$

The coarse-grained function of generalized Lyapunov coefficients  $(q)$  is given by  $(q) = \int d(q) = dq$  and the variance  $v(q)$  of  $P(\lambda; t)$  by  $v(q) = \int d(q) = dq$  [23], [21], [22]. The functions  $(q)$  and  $(\cdot)$  are the dynamic counterparts of the Renyi dimensions  $D(q)$  and the spectrum  $f(\cdot)$  that characterize the geometric structure of the attractor [2]. The form  $t^{-(1)}$  for  $P(\lambda; t)$  and the weight  $t^{(q-1)\lambda}$  in Eq. (24) are intended for the description of the envelope of the fluctuations at the critical attractor [23], [21], [22].

As with ordinary thermal first order phase transitions, a 'q-phase' transition is indicated by a section of linear slope  $m_c = 1 - q$  in the spectrum (free energy)  $(\cdot)$ , a discontinuity at  $q = q$  in the Lyapunov function (order parameter)  $(q)$ , and a divergence at  $q$  in the variance (susceptibility)  $v(q)$ . For the onset of chaos at golden mean a single  $q$ -phase transition was numerically determined [23] and found to occur approximately at a value around  $m_c = (1 - q)' = 0.95$ . It was pointed out in Ref. [23] that this value would actually be  $m_c = (1 - q) = \max_{q=2} = 0.948997$ . Our analysis below shows that this initial result gives a rough picture of the dynamics at the golden mean attractor and that actually an infinite family of  $q$ -phase transitions of decreasing magnitude takes place there.

From the results for  $\frac{(k)}{q}$  and  $\frac{(k)}{2-q}$  we can construct the two-step Lyapunov function

$$(q) = \begin{cases} < \frac{(1)}{q}; & 1 < q < q; \\ 0; & q < q < 2 - q; \\ > \frac{(1)}{2-q}; & 2 - q < q < 1; \end{cases} \quad (25)$$

where  $\frac{(1)}{q} = 2 \ln j_{gm} = \ln w_{gm} = 1.053744$  and  $\frac{(1)}{2-q} = w_{gm}^{-1} \frac{(1)}{q} = 1.704994$ . See Fig. 5a. Direct contact can be established now with the formalism developed by Mori and coworkers and the  $q$ -phase transition reported in Ref. [21]. The step function for  $(q)$  can be integrated to obtain the spectrum  $(q) = \int d(q) = dq$  and from this its Legendre transform  $(\cdot) = (1 - q)$ . The free energy functions  $(q)$  and  $(\cdot)$  obtained from the two-step  $(q)$  determined above are given by

$$(q) = \begin{cases} < \frac{(1)}{q} (q - q); & q < q; \\ 0; & q < q < 2 - q; \\ > \frac{(1)}{2-q} (q - 2 + q); & q > 2 - q; \end{cases} \quad (26)$$

and

$$(\cdot) = \begin{cases} (1 - q); & \frac{(1)}{2-q} < \cdot < 0; \\ (1 - q); & 0 < \cdot < \frac{(1)}{q}; \end{cases} \quad (27)$$

See Fig. 5b. The constant slopes of  $(\cdot)$  represent the  $q$ -phase transitions associated with trajectories linking two

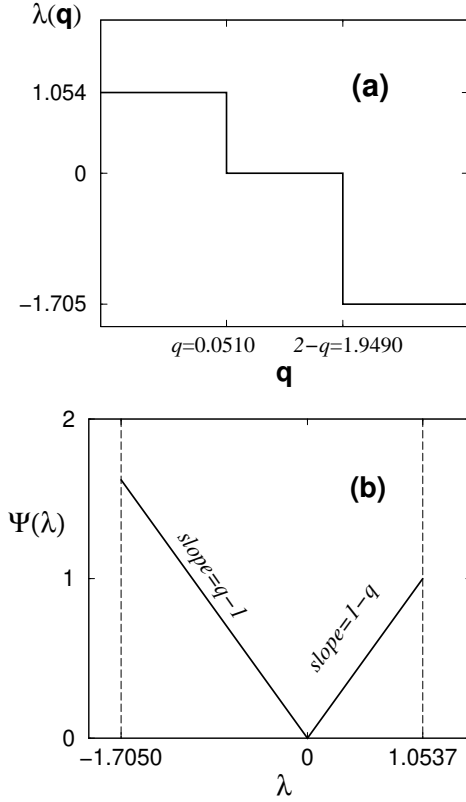


FIG. 5:  $q$ -phase transitions occurring at index values  $q$  and  $2 - q$ . (a) The two-step Lyapunov function  $\lambda(q)$ . (b) The piece-wise spectrum  $\Psi(\lambda)$ . These transitions correspond to the main discontinuity in the trajectory scaling function  $\chi(y)$ . See text for details.

regions of the attractor,  $y' = 0$  (or  $y' = 1$ ) and  $y' = 1 - y$ , and their values  $1 - q$  and  $q - 1$  correspond to the index  $q$  obtained for the  $q$ -exponentials  $\chi_t$  in Eqs. (17) and (20). The slope  $q - 1 = \chi_{m_{ax}=2} = 0.949$  coincides with that originally detected in Ref. [21].

## VI. MULTIFRACTAL DYNAMICS FROM THE TRAJECTORY SCALING FUNCTION

The trajectory scaling function  $\chi(y)$  for the golden mean route is constructed [25], [26] via the evaluation of the ratios

$$\chi_n(m) = \frac{d_{n+1,m}}{d_{n,m}}; \quad (28)$$

where  $d_{n,m} = j_m - F_n + m$ ,  $j_m = 0; 1; 2; \dots$ , and where the denominator is replaced by  $d_{n,m} = j_m - m - F_n$  in case  $m = F_n$ . The function  $\chi(y)$  is obtained as the limit  $\chi(y) = \lim_{n \rightarrow \infty} \chi_n(m)$  where  $y = \lim_{n \rightarrow \infty} (m - F_n) = F_n$ , and shows finite (jump) discontinuities at all rationals of the form  $m = F_n$ . The main discontinuity appears at  $y = 0$ , since  $\chi(0) = j_{gm} j^1$  but  $\chi(0^+) = j_{gm} j^3$ , and again at  $y = w_{gm}^2$ . Other discontinuities in  $\chi(y)$  appear at

$y = w_{gm}, w_{gm}^3, w_{gm}^4, w_{gm} + w_{gm}^3, w_{gm} + w_{gm}^4$ , etc., and of course  $w_{gm} + w_{gm}^2 = 1$ . We leave a detailed account of these properties to a later occasion [29]. In most cases it is only necessary to consider the first few as their magnitude decreases rapidly. See, e.g. Fig. 2 in Ref. [26]. The discontinuities of  $\chi_n(m)$  can be suitably obtained by first generating the superstable orbit at  $y = 1$  and then plotting the position differences  $j_m - j$  for times of the form  $m = F_n + m$ ,  $n = 0; 1; 2; \dots$ , in logarithmic scales. The distances that separate positions along the time subsequence correspond to the logarithm of the distances  $d_{n,m}$ . See Figs. 3 and 4 where the constant spacing of positions along the main diagonal provide the values for  $\ln d_{n,0} = n \ln j_{gm} j$  and  $\ln d_{n,1} = 3n \ln j_{gm} j$  respectively. The constant slope  $s_m$  of the resulting time subsequence data is related to  $\chi_n(m)$ , i.e.  $\chi_n(m) = (w_{gm})^{s_m}$ . See Figs. 3 and 4 where the slopes of the main diagonal subsequences have the values  $\ln j_{gm} j = \ln w_{gm}$  and  $3 \ln j_{gm} j = \ln w_{gm}$ , respectively. From these two slopes the value of the largest jump discontinuity of  $\chi_n(m)$  is determined.

The sensitivity  $\chi_t(0)$  can be evaluated for trajectories within the attractor via consideration of the discontinuities of  $\chi(y)$ . We set the initial and the final separation of the trajectories to be the diameters  $\chi(0) = d_{n,m}$  and  $\chi(t) = d_{n,m} + t$ ,  $t = F_n - 1$ , respectively. Then,  $\chi_t(0)$  is obtained as

$$\chi_t(0) = \lim_{n \rightarrow \infty} \frac{d_{n,m} + t}{d_{n,m}}; \quad (29)$$

Notice that in this limit  $\chi(0) \neq 0$ ,  $t \neq 1$  and the  $F_n$ -supercycle becomes the onset of chaos. Then,  $\chi_t(0)$  can be written as

$$\chi_t(m) = \frac{\chi_n(m-1)^n}{\chi_n(m)}; \quad t = F_n - 1 \text{ and } n \text{ large}; \quad (30)$$

where we have used  $j_n(m) j^n = \prod_{i=1}^n j_{i+1,m} = d_{i,m} j$  and  $d_{i+1,m} + F_n = d_{i+1,m}$ . Notice that for the inverse process, starting at  $\chi(0) = d_{n,m} + t = d_{n,m} - 1$  and ending at  $\chi(t^0) = d_{n,m} = d_{n,m} - 1 + t^0$ , with  $t^0 = F_n + 1$  one obtains

$$\chi_{t^0}(m-1) = \frac{\chi_n(m)}{\chi_n(m-1)^n}; \quad t^0 = F_n + 1 \text{ and } n \text{ large}; \quad (31)$$

Therefore, from the properties of  $\chi(y)$  we can determine those for  $\chi_t$ . This function can be obtained at different levels of approximation by considering only a fixed number of its larger discontinuities. The discontinuities of  $\chi(y)$  appear divided into two sets, the first falls on the interval  $0 < y < w_{gm}$ , and the second on  $w_{gm} < y < 1$ . The amplitudes of the jumps in the second set are much smaller than those in the first set [26]. The simplest approximation for  $\chi(y)$  is to consider only one jump in the first set at  $w_{gm}^2$  and none in the second set, so that

$$\chi(y) = \begin{cases} 0^1; & 0 < y < w_{gm}^2; \\ 1^1; & w_{gm}^2 < y < 1; \end{cases} \quad (32)$$

where  $\alpha_0 = j_{gm} j^3$ ,  $\alpha_1 = j_{gm} j^2$ ,  $\alpha_2 = j_{gm} j$ ,  $\alpha_3 = 1$ . This level of approximation assumes that there are only two scaling factors, those corresponding to the most crowded and most sparse regions of the attractor. The next level of approximation for  $(y)$  involves two jumps in the first set at  $w_{gm}^3$  and  $w_{gm}^2$ , and still none in the second set, so that

$$(y) = \begin{cases} 0^1; 0 & Y < w_{gm}^3; \\ 1^1; w_{gm}^3 & Y < w_{gm}^2; \\ 2^1; w_{gm}^2 & Y < w_{gm}^1; \\ 3^1; w_{gm}^1 & Y < 1 \end{cases} \quad (33)$$

where  $\alpha_0 = j_{gm} j^3$ ,  $\alpha_1 = j_{gm} j^2$ ,  $\alpha_2 = j_{gm} j$ ,  $\alpha_3 = 1$ . The two additional scaling factors correspond to two 'medium' regions between the most crowded and most sparse regions of the attractor. More accurate approximations to  $(y)$  can be constructed by incorporation of additional discontinuities. Note that the number of discontinuities increase in each set as  $F_M \rightarrow 1$ ,  $M = 1; 2; \dots$

Use of Eq. (32) in Eqs. (30) and (31) (together with Eq. (16)) recovers our previous results for  $t$  and  $q$  in Eqs. (17) to (21), and therefore also those for  $(q)$ ,  $(q)$  and  $(\cdot)$  in Eqs. (25) to (27). When use is made of Eq. (33) in Eqs. (30) and (31) we obtain three values for the  $q$  index,  $q_0$ ,  $q_1$  and  $q_2$  (together with the conjugate values  $2 - q_0$ ,  $2 - q_1$  and  $2 - q_2$  for the inverse trajectories). For each value of  $q$  there is a set of  $q$ -Lyapunov coefficients running from a maximum  $q_{j, \max}$  to zero (or a minimum  $q_{j, \min}$  to zero). From the results for  $q_j^{(k)}$  and  $2 - q_j^{(k)}$ ,  $j = 0; 1; 2$ , we can construct three Lyapunov functions  $j(q)$ ,  $1 < q < 1$ , each with two jumps located at  $q = q_j = 1 - \ln 2 = \ln j = j+1$  and  $q = 2 - q_j$ . We obtain a couple of two  $q$ -phase transitions for each of the three values of the  $q$  index,  $q_0$ ,  $q_1$  and  $q_2$ . The constant slope values for the  $q$ -phase transitions at  $1 - q_0$  and  $q_0 - 1$  appear again, but now we have two other pairs of transitions with slope values  $1 - q_1$  and  $q_1 - 1$ , and,  $1 - q_2$  and  $q_2 - 1$ , that correspond, respectively, to orbits that link the most crowded region of the attractor to the 'medium crowded' region, and to orbits that link the 'medium sparse' region with the 'most sparse' region of the attractor. Similar but more elaborated results are obtained when more discontinuities in  $(y)$  are taken into account. These results reflect the multi-region nature of the multifractal attractor and the memory retention of these regions in the dynamics. Thus, when  $(y) = (y+)$  one has  $t = 1$  (or  $q(0) = 0$ ) which corresponds to trajectories that depart and arrive in the same region, when  $(y) \neq (y+)$  the power laws in Eqs. (30) and (31) correspond to a departing position in one region and arrival at a different region and vice versa, the trajectories expand in one sense and contract in the other.

## VII. SUMMARY AND ASSESSMENT OF APPLICABILITY OF $q$ -STATISTICS

We have examined in detail the structure of the superstable orbit at the golden mean critical attractor for zero-slope cubic inflection point maps. The knowledge of this structure allowed us to determine the sensitivity to initial conditions for sets of starting positions within the attractor. We found that  $t$  is made up of a hierarchy of families of infinitely many interconnected  $q$ -exponentials. Each pair of regions in the multifractal attractor, that contain the starting and finishing positions of a set of trajectories, leads to a family of  $q$ -exponentials with a fixed value of the index  $q$  and an associated spectrum of  $q$ -Lyapunov coefficients  $q^{(k)}$ . The indexes  $q$  and the spectra  $q^{(k)}$  come in pairs,  $q$  and  $2 - q$ , and  $q^{(k)}$  and  $2 - q^{(k)}$ , as these correspond to switching starting and finishing trajectory positions. This dynamical organization is difficult to resolve from the consideration of a straightforward time evolution, i.e. the record of positions at every time  $t$  for a trajectory started at an arbitrary position  $(0)$  within the attractor. In this case what is observed [21] are strongly fluctuating quantities that persist in time with a scrambled pattern structure that exhibits memory retention. Unsystematic averages over  $(0)$  would rub out the details of the multiscale dynamical properties we uncovered. On the other hand, if specific initial positions with known location within the multifractal are chosen, and subsequent positions are observed only at pre-selected times, when the trajectories visit another selected region, a distinct  $q$ -exponential expression for  $t$  is obtained.

Subsequently, we explained that the above described properties for the sensitivity relate to sets of dynamical phase transitions. That is, the dynamics on the attractor consists of an infinite family of Mori's  $q$ -phase transitions, each associated, as before, to trajectories that have common starting and finishing positions located at specific regions of the attractor. The specific values of the variable  $q$  in the formalism of Mori and colleagues at which the  $q$ -phase transitions take place are the same values for the Tsallis entropic index  $q$  in  $t$ . The transitions come in pairs at  $q$  and  $2 - q$  as they are tied down to the expressions for  $q^{(k)}$  in  $t$ . The dominant dynamical transition is associated with movement from the most crowded to the most sparse regions of the attractor (or vice versa) and the values of its relevant parameters coincide with those found in an earlier study with the use of Mori's formalism [21]. Here we have determined the  $q$ -phase transitions via the direct evaluation of the spectra  $q^{(k)}$  and  $2 - q^{(k)}$  in  $t$ . Also, we established a connection between the trajectory scaling function and the expressions for  $t$ , such that the discontinuities of the former determine the  $q$ -phase transitions and the values for the  $q$  index. Conversely, from the  $q$ -exponential expressions for  $t$  the scaling function can be conveniently determined.

Our results clearly apply to many other families of



maps with zero slope in action points of cubic nonlinearity and are likely to hold also for general nonlinearity  $z > 1$  [30]. These results may be of relevance in condensed matter problems where the quasiperiodic route to chaos is involved. One interesting example is the phenomenon of the localization transition for transport in incommensurate systems, where Schrödinger equations with quasiperiodic potentials [31] are equivalent to nonlinear maps with a quasiperiodic route to chaos, and where the divergence of the localization length translates into the vanishing of the ordinary Lyapunov coefficient [32]. The dynamics at this type of multifractal critical attractor is also represented by a  $t$  given by families of interconnected  $q$ -exponentials with  $q$ -generalized spectra of Lyapunov coefficients  $\lambda_q^{(k)}$ . The latter quantities yield information on the power-law decay rates of multifractal-structured wave functions at the localization transition. Our findings reported here are very similar to those recently determined for the Feigenbaum attractor in unimodal maps [15], and reinforce the notion of generality of our identification of the source for the entropic index  $q$  observed at critical attractors.

#### A. The utility of $q$ -statistics

Before concluding our analysis it is of interest to reconsider our developments in such a way as to illustrate the incidence and usefulness of the  $q$ -statistics in the description of the dynamics on the attractor at the transition to chaos. We return to the dynamical partition function in Eq. (24) and rewrite it as

$$Z(\epsilon; q) = \int dP(\epsilon; \epsilon) W(\epsilon; \epsilon)^{1/q}; \quad (34)$$

where the weight  $W(\epsilon; \epsilon)$  was assumed by Mori and colleagues [23] to have the form  $W(\epsilon; \epsilon) = \exp(\epsilon)$  for chaotic attractors and  $W(\epsilon; \epsilon) = 1$  for the envelope of fluctuations of the attractor at the onset of chaos, with a generalized Lyapunov coefficient. The variable  $q$  plays the role of a 'thermodynamic field' like the external magnetic field in a thermodynamic system, alternatively,  $1/q$  can be thought analogous to the inverse temperature. We note that  $W(\epsilon; \epsilon)$  can be written in both cases as

$$W(\epsilon; \epsilon) = \frac{df^{(\epsilon)}(\epsilon)}{d\epsilon} \quad (35)$$

since  $\epsilon(\epsilon; 0) = A(\epsilon) \ln df^{(\epsilon)}(\epsilon) = d\epsilon$  with  $A(\epsilon) = 1$  for chaotic attractors and  $A(\epsilon) = (\ln \epsilon)^{-1}$  for the envelope of the fluctuating sensitivity of the critical attractor [23]. For chaotic attractors the fluctuations of  $\epsilon(\epsilon; 0)$  die out as  $\epsilon \rightarrow 1$  and this quantity becomes the ordinary Lyapunov coefficient  $\lambda_1$  independent of the initial position  $\epsilon_0$ . For critical attractors  $\epsilon(\epsilon; 0)$  maintains its dependence on  $\epsilon$  and  $\epsilon_0$  but as we have seen  $\epsilon(\epsilon; 0)$  is a well-defined constant provided  $\epsilon$  takes values from a time

subsequence  $(n; k; l)$ , as explained in Sections 3 and 4 and shown in Figs. 3 and 4. For simplicity we consider now only the case  $l = 0$ , i.e. the subsequences  $(n; k) = kF_n$ ,  $n = 1; 2; 3; \dots$  for fixed values of  $k = 1; 2; 3; \dots$ , but it is important to note that every natural number appears in the complete set of subsequences. One branch of the envelope of  $\epsilon$  with  $\epsilon_0 = 0$  is visited at times of the form  $\epsilon = F_n$  for which we find  $\epsilon(F_n; 0) = \lambda_q^{(1)}$  while for other time subsequences one has  $\epsilon(kF_n; 0) = \lambda_q^{(k)}$  (see Eq. (19)). Again for simplicity we ignore the inverse trajectories that lead to the conjugate  $\lambda_{2-q}^{(k)}$  (see Eq. (21)).

As we have proved, along each time subsequence the sensitivity  $\epsilon = df^{(\epsilon)}(\epsilon) = d\epsilon$  is given by a  $q$ -exponential, like in Eq. (15), and consequently we can express  $\epsilon(\epsilon; 0)$  in terms of the  $q$ -deformed logarithm  $\epsilon(\epsilon; 0) = \lambda_q^{-1} \ln_q df^{(\epsilon)}(\epsilon) = d\epsilon$  with  $q$  given by e.g. Eq. (18). Therefore for times of the form  $(n; k) = kF_n$  we have

$$P(\epsilon; \epsilon) W(\epsilon; \epsilon) = \lambda_q^{(k)} \exp_q(\lambda_q^{(k)} \epsilon); \quad (36)$$

with  $\epsilon = k$ , and

$$Z(\epsilon; q) = W(\epsilon; \epsilon)^{1/q} = \frac{1}{1 + (1 - q) \lambda_q^{(k)} \epsilon^{(1-q)}}; \quad (37)$$

Notice that in Eq. (37)  $q$  is a running variable while  $\epsilon$  is fixed as in Eq. (18).

The next step is to consider the uniform probability distribution, for fixed  $\lambda_q^{(k)}$  and  $\epsilon$ , given by  $p_i(\lambda_q^{(k)}; \epsilon) = \bar{W}^{-1}$ ,  $i = 1; \dots; \bar{W}$ , where  $\bar{W}$  is the integer nearest to (a large)  $W$ . A trajectory starting from  $\epsilon_0 = 0$  visits a new site belonging to the time subsequence  $\epsilon = kF_n$  every time the variable  $n$  increases by one unit and never repeats one. Each time this event occurs phase space is progressively covered with an interval  $\epsilon_n = kF_{n+1} - kF_n$ . The difference of the logarithms of the times between any two such consecutive events is the constant  $\ln \lambda_{gm}^{-1}$ ,  $n$  large, whereas difference of the logarithms of the corresponding phase space distances  $kF_{n+1}$  and  $kF_n$  is the constant  $2 \ln j_{gm}$ . We define  $W_n$  to be the total phase space distance covered by these events up to time  $\epsilon = kF_n$ . In logarithmic scales this is a linear growth process in space and time from which the constant probability  $\bar{W}_n^{-1}$  of the uniform distribution  $p_i$  is defined. In ordinary phase space and time we obtain instead  $W^{-1} = \exp(-\lambda_q^{(k)} \epsilon)$ . We then have that

$$Z(\epsilon; q) = \sum_{i=1}^{\bar{W}} p_i^q = 1 + (1 - q) S_q; \quad (38)$$

where  $S_q = \ln_q \bar{W}$  is the Tsallis entropy for  $p_i$ .

The usefulness of the  $q$ -statistical approach is now evident when we recall from our discussion in the previous section that the dynamics on the critical attractor is constituted (in its entirety) by a discrete set of  $q$ -phase

transitions and that at each of them the field variable  $q$  takes a specific value  $q = q_i$ . At each such transition both  $Z$  and  $S_q$  grow linearly with time along the subsequences  $(n; k)$ . In addition,  $\tau_q^{(k)}$  can be determined from  $S_q = t = \tau_q^{(k)}$ . Thus, with the knowledge we have gained,

a convenient procedure for determining the actuating dynamics at a critical multifractal attractor could take advantage of the above properties.

Acknowledgments. Partially supported by CONACyT and DGAPA-UNAM, Mexican agencies.

- 
- [1] H.G. Schuster, Deterministic Chaos. An Introduction, 2nd Revised Edition (VCH Publishers, Weinheim, 1988).
- [2] C. Beck and F. Schlögl, Thermodynamics of Chaotic Systems (Cambridge University Press, UK, 1993).
- [3] R.C. Hilborn, Chaos and nonlinear dynamics, 2nd Revised Edition (Oxford University Press, New York, 2000).
- [4] C. Tsallis, A.R. Plastino and W.-M. Zheng, Chaos, Solitons and Fractals 8, 885 (1997).
- [5] M.L. Lyra and C. Tsallis, Phys. Rev. Lett. 80, 53 (1998).
- [6] U. Timakli, C. Tsallis and M.L. Lyra, Eur. Phys. J. B 11, 309 (1999).
- [7] F.A.B.F. de Moura, U. Timakli and M.L. Lyra, Phys. Rev. E 62, 6361 (2000).
- [8] F. Baldovin and A. Robledo, Phys. Rev. E 66, 045104 (R) (2002).
- [9] F. Baldovin and A. Robledo, Phys. Rev. E 69, 045202 (R) (2004).
- [10] E. Mayoral and A. Robledo, Physica A 340, 219 (2004).
- [11] A. Robledo, Physica D 193, 153 (2004).
- [12] F. Baldovin and A. Robledo, Europhys. Lett. 60, 518 (2002).
- [13] A. Robledo, Molec. Phys. 103, 3025 (2005).
- [14] A. Robledo, Phys. Lett. A 328, 467 (2004); F. Baldovin and A. Robledo, cond-mat/0504033.
- [15] E. Mayoral and A. Robledo, Phys. Rev. E 72, 026209 (2005).
- [16] C. Tsallis, J. Stat. Phys. 52, 479 (1988).
- [17] For recent reviews see, Nonextensive Entropy { Interdisciplinary Applications, M. Gell-Mann and C. Tsallis, eds., (Oxford University Press, New York, 2004). See <http://tsallis.cat.cbpf.br/biblio.htm> for full bibliography.
- [18] C. Grebogi, E. Ott, S. Pelikan, and J.A. Yorke, Physica D 13, 261 (1984).
- [19] P. Grassberger and M. Scheunert, J. Stat. Phys. 26, 697 (1981).
- [20] G. Anania and A. Politi, Europhys. Lett. 7, 119 (1988). This work headed the determination of the spectrum of anomalous Lyapunov coefficients at the onset of chaos in the logistic map.
- [21] T. Horita, H. Hata, H. Mori and K. Tomita, Prog. Theor. Phys. 81, 1073 (1989).
- [22] H. Hata, T. Horita and H. Mori, Prog. Theor. Phys. 82, 897 (1989).
- [23] H. Mori, H. Hata, T. Horita and T. Kobayashi, Prog. Theor. Phys. Suppl. 99, 1 (1989).
- [24] M.J. Feigenbaum, Commun. Math. Phys. 77, 65 (1980); Physica 7D, 16 (1983).
- [25] M.J. Feigenbaum, in Proceedings of the 1984 Latin American School of Physics, Santiago, Chile, F. Claro, Editor (Springer-Verlag, Berlin, 1985).
- [26] R. Mainieri, Phys. Rev. E 48, 898 (1993); R. Mainieri and R.E. Ecke, Physica D 79, 193 (1994).
- [27] M.H. Jensen, L.P. Kadano, A. Libchaber, I. Procaccia and J. Stavans, Phys. Rev. Lett. 55, 2798 (1985).
- [28] M.J. Feigenbaum, L.P. Kadano and S.J. Shenker, Physica 5D, 370 (1982).
- [29] H. Hernandez-Saldana and A. Robledo, in preparation.
- [30] R. Delbourgo and B.G. Kenny, Phys. Rev. A 42, 6230 (1990).
- [31] P.G. Harper, Proc. Phys. Soc., London, Sect. A 68, 874 (1955).
- [32] J.A. KETOJA and I.I. Satiya, Physica D 109, 70 (1997).